Journal of the Optical Society of America A
OPTICS, IMAGE SCIENCE, AND VISION

# The partial light scattering cross section of spherical particles

CHRISTOPHER M. SORENSEN,* JUSTIN B. MAUGHAN, AND AMITABHA CHAKRABARTI

*Department of Physics, Kansas State University, Manhattan, Kansas 66502, USA*
**Corresponding author: sor@phys.ksu.edu*

*Received 23 November 2016; revised 20 February 2017; accepted 14 March 2017; posted 14 March 2017 (Doc. ID 281354); published 4 April 2017*

**We define the partial scattering cross section and partial efficiencies to demonstrate that the total scattering is the sum of two roughly equal parts: approximately half from the forward scattering lobe due to 2D diffraction by the projected sphere and half from the 2D to 3D diffraction crossover. The first part is at angles such that $\theta \lesssim \lambda/D$, a result previously known, which can be quite small for large particles. The second part is in a new regime we call the "hump," visible in q-space, which to a good approximation contains the other half of the scattered light. The hump disappears when the imaginary part of the refractive index is significant.** 

***OCIS codes:*** (290.0290) Scattering; (290.4020) Mie theory; (290.5825) Scattering theory.

https://doi.org/10.1364/JOSAA.34.000681

The angular distribution of light scattered by a particle is an important scientific subject. It is typically described by the differential cross section or the phase function, which is a doubly normalized version of that cross section. This cross section is ideal for describing light scattered energy to a detector at an angular position $(\varphi, \theta)$ subtending a certain solid angle.

The purpose of this paper is to present another way of quantitatively describing the distribution of scattering which leads to a refined sense of at what angles the scattered light is most distributed. Consider a simple scattering arrangement in which unpolarized light is incident along the positive $z$-axis and encounters a particle. The total scattering cross section is the integral of the differential cross section over the entire $4\pi$ steradians. Given this and our desire to study the distribution of scattering, we seek a cumulative fraction of the total scattering cross section with varying degrees of the solid angle. The integration will start at the forward direction, $\theta = 0$, and proceed to a finite $\theta_p$. For any given $\theta_p$, the entire $\varphi$ range integration of $0 - 2\pi$ is performed. Thus we define the *partial scattering cross section*, $\partial C_{\mathrm{sca}}(\theta_p)$, as

$$\partial C_{\mathrm{sca}}(\theta_p) = \int_0^{\theta_p} \int_0^{2\pi} \mathrm{d}C_{\mathrm{sca}}/\mathrm{d}\Omega \mathrm{d}\varphi \sin\theta \mathrm{d}\theta. \tag{1}$$

A similar integral was used to study nephelometer truncation errors in [1]. Figure 1 shows a diagram of $\partial C_{\mathrm{sca}}(\theta_p)$. The partial scattering cross section shows how the total scattering accumulates with increasing scattering angle $\theta$. It follows that at $\partial C_{\mathrm{sca}}(180°) = C_{\mathrm{sca}}$, the total scattering cross section.

Our study of the partial cross section will be confined to spherical particles of radius $R$. We will use Q-space analysis, so a brief description of this analysis is given here. Q-space analysis involves plotting the scattered intensity, as embodied in the differential scattering cross section and proportional to the phase function, versus the dimensionless variable $qR$, where $q$ is the magnitude of the scattering wave vector, $q = (4\pi/\lambda)\sin(\theta/2)$, where $\lambda$ is the wavelength of light [2]. The plot is double logarithmic. Q-space analysis reveals functionalities of the scattering with q that are not apparent with conventional plotting with the scattering angle. Often in Q-space analysis, the differential cross section is normalized by the particle's Rayleigh differential cross section given by

$$dC_{\mathrm{sca,Ray}}/d\Omega = k^4 R^6 F(m), \tag{2}$$

where $k = 2\pi/\lambda$,

$$F(m) = \left|\frac{m^2 - 1}{m^2 + 2}\right|^2 \tag{3}$$

is the square of the Lorentz–Lorenz factor, and $m = n + i\kappa$ is the complex refractive index of the particle. Plots of the Rayleigh normalized scattering in q-space for different spheres closely align when their internal coupling parameters are equal. The internal coupling parameter $\rho'$ is given by [3]

$$\rho' = 2kR\sqrt{F(m)} = 2kR\left|\frac{m^2 - 1}{m^2 + 1}\right|. \tag{4}$$

Figure 2 considers scattering of unpolarized light with wavelength $\lambda = \pi/6\ \mu\mathrm{m} = 0.524\ \mu\mathrm{m}$ by spheres with three different real refractive indices and three different radii such that all three have the same internal coupling parameter $\rho' = 100$. The lower half of Fig. 2 contains the Rayleigh normalized differential scattering cross section versus $qR$. Note that these plots for the three different sizes and three different refractive indices (but

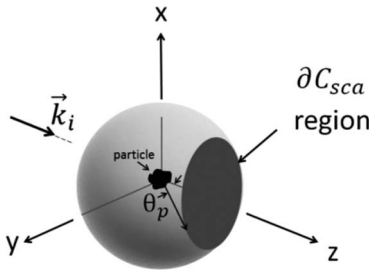


**Fig. 1.** Diagram of light incident upon an arbitrary particle. The light scattered at angles less than $\theta_p$ symmetrically around the $z$-axis (darkened area) is included in the partial scattering cross section, $\partial C_{\mathrm{sca}}(\theta_p)$.

same $\rho'$) align well with each other except near the large end when $qR = 2kR$ where enhanced backscattering including the glory exists. Also note that when $qR < 1$, the scattering is essentially constant; this is the forward scattering lobe. At larger $qR$ a brief regime occurs with a $(qR)^{-3}$ envelop, which is the 2D Fraunhofer diffraction regime due to the fact that spheres with large $\rho'$ can act as circular obstacles for the light [4]. At yet larger $qR$, the two-dimensional diffraction gives way to a "hump" centered near $\rho'$. This hump leads the scattering to join roughly the Rayleigh–Debye–Gans (RDG) limit, which is what the scattering would be if $\rho' \ll 1$. This RDG limit is also the 3D diffraction limit of the sphere given by the square of the Fourier transform of a sphere.

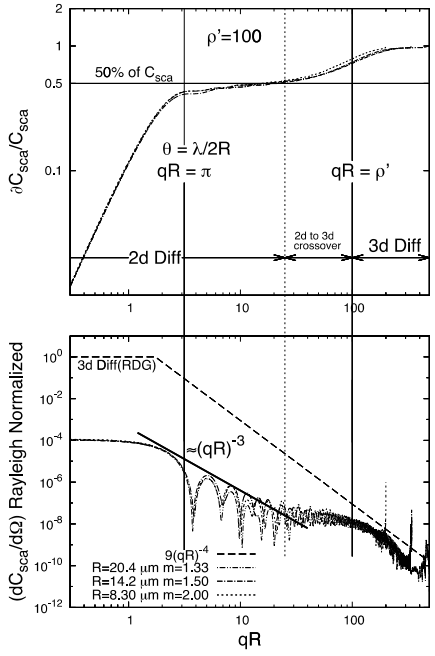


**Fig. 2.** Lower half is a q-space plot of the Rayleigh normalized differential scattering cross section versus the dimensionless $qR$ with $\theta = \theta_p$ for three spheres scattering light with a wavelength of $\pi/6$ μm = 0.524 μm, all with a real refractive index and the same internal coupling parameter $\rho' = 100$. Upper half shows the normalized partial scattering cross section for the same three spheres ($qR$ scale matched with the lower half). Regimes of 2D and 3D diffraction are indicated as well as where the scattering angle $\theta = \lambda/2R$.

The upper half of Fig. 2 shows the normalized partial scattering cross section, $\partial C_{\mathrm{sca}}/C_{\mathrm{sca}}$, versus $qR$, with $\theta = \theta_p$, and the $qR$ scales are matched between the two halves. This comparison shows that the normalized partial scattering cross section initially increases rapidly with $qR$, i.e., it increases rapidly as more of the forward scattering is included. Comparison to the lower half shows that this rapid increase occurs in the forward scattering lobe. The increase levels off at a value quite close to ½ near $qR = \pi$, which corresponds to an angle of $\theta_p = \lambda/2R = \lambda/D$. After that, $\partial C_{\mathrm{sca}}/C_{\mathrm{sca}}$ remains roughly constant until $qR$ reaches a value that the lower graph marks as the end of the −3 power law of the 2D circular aperture diffraction regime. Then it begins a slow rise as the hump begins, the middle of which is near $qR \simeq \rho'$. The rise stops and $\partial C_{\mathrm{sca}}/C_{\mathrm{sca}}$ approaches unity as $qR$ begins to approach the RDG regime indicative of 3D spherical particle diffraction.

To summarize:

1. The partial scattering cross section, $\partial C_{\mathrm{sca}}$, is ∼50% the total scattering cross section by end of forward scattering lobe, which is at $qR = \pi$, corresponding to $\theta = \lambda/2R = \lambda/D$.
2. The second ∼50% is accumulated in the hump, which is the 2D–3D Fraunhofer diffraction crossover centered near $qR \simeq \rho'$.
3. The partial scattering cross section behavior with $q$ (hence $\theta$) is essentially universal with $\rho'$.

Figure 3 shows the partial scattering cross section for a smaller sphere with a radius of $R = 3$ μm and a real refractive index of $m = 1.5$ scattering 0.524 μm light, hence $\rho' = 21.2$. For such a particle the 2D and 3D diffraction regions are not as well defined as for the larger particles examined in Fig. 2. Nevertheless, the conclusions are the same for this $\rho' = 21.2$: approximately half the light is scattered in the forward lobe; there is then a brief pause followed by the other half accumulated around the regions

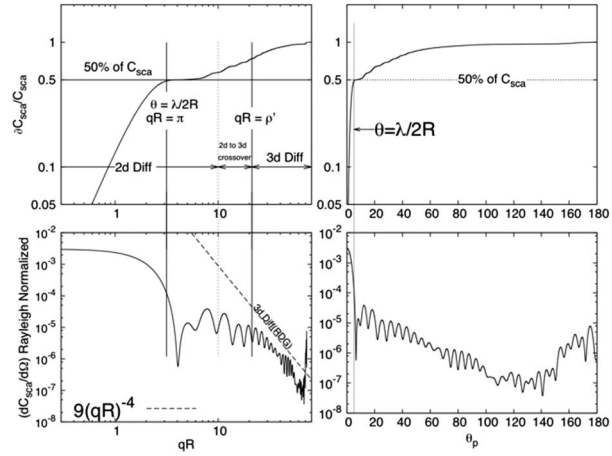


**Fig. 3.** Example for a sphere of radius $R = 3$ μm and real refractive index $m = 1.5$ scattering light with a wavelength of $\pi/6$ μm = 0.524 μm. This leads to $\rho' = 21.2$. Lower halves are plots of the Rayleigh normalized differential scattering cross section versus the dimensionless $qR$ (left) or the scattering angle $\theta$ (right). Upper halves show the normalized partial scattering cross section for the same independent variables.

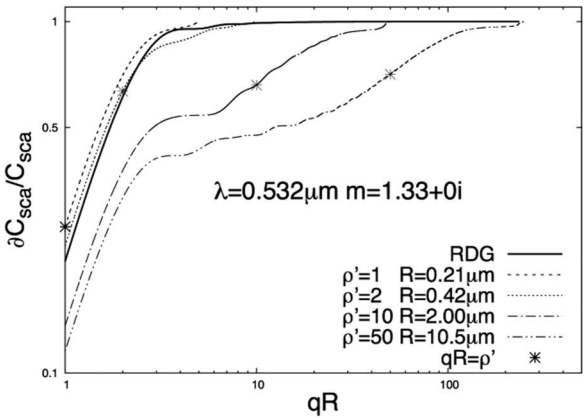


**Fig. 4.** Normalized partial cross section versus $qR$ for a sphere with refractive index $m = 1.33$ and variety of sizes and hence different internal coupling parameters to demonstrate the behavior as $\rho' \to 0$.

where $qR \simeq \rho'$. The behavior of the partial cross section for yet smaller particles is described in reference to Fig. 4, below.

Figure 3 also compares the Q-space analysis to the conventional plot versus the scattering angle $\theta$ and thereby explicitly demonstrates a crucial message that about half of all the scattered light is in the narrow forward scattering lobe for which $\theta \leq \lambda/D$. In this example of $D = 6$ μm, approximately half of all the scattered light is in angles $\theta \leq 6°$. The other half is in the hump, which is not so obvious in theta space, between ∼11° and 80°.

The forward scattering half is well known. Some time ago Brillouin [5] studied the scattering cross section for large spheres with regard to the fact that the total scattering cross section for such spheres is twice the projected geometric cross section, the so-called extinction paradox. He found that to within a few percent half the light energy was scattered at angles less than $\theta \simeq 3\lambda/R$ and the second half was scattered in the range greater than this angle out to $\theta = \pi$ (180°). Borovoi [6] used the physical optics approximation for particles of arbitrary shapes to show that approximately half the scattered light is in the forward scattering lobe defined by the Fraunhofer diffraction from the particle. These results are supported by the geometric optics approximation for large particles that demonstrates that refraction, reflection, and absorption can contribute one geometric cross section to the total extinction cross section, leaving diffraction to contribute another geometric cross section, hence another half, into the forward cone [7,8]. More recently, we have stressed the importance of this forward scattering lobe in experimental measurements of light scattering [9,10]. What is new in our work here is the identification of the hump visible in q-space, which to a good approximation contains the other half of the scattered light.

Close examination of the differential scattering cross section in the lower halves of Figs. 2 and 3 shows that the scattering for a large, refractive sphere (as indicated by large $\rho'$) is broken up into three major regimes listed here in order of increasing $qR$: 2D Fraunhofer diffraction (which includes the forward scattering lobe), 3D Fraunhofer diffraction (which includes the hump), enhanced backscattering. The partial scattering cross section indicates that approximately half of the total scattering occurs in each of the two diffraction regimes. Moreover, these halves are dominated by their forward lobes, the forward lobe for 2D diffraction being when $qR \leq \pi$ and for 3D diffraction the hump approximately when $\frac{1}{2}\rho' \lesssim qR \lesssim 2\rho'$. The subsequent (and rough) −3 and −4 power laws after these forward lobes add very little to the total scattering, as is also true of the enhanced backscattering.

Figure 4 explores the functionality of the partial scattering cross section on $\rho'$, as the particles and hence $\rho'$ become small and pass into the RDG limit. For large $\rho'$ the roughly equal division of total scattering between the 2D and 3D diffraction regimes endures. In the RDG limit, as $\rho' \to 0$, the 2D diffraction regime disappears, and the 3D diffraction dominates the scattering. In this limit nearly all the light is scattered in the forward lobe, which for small particles is broad. Figure 4 shows again that the center of the hump, hence the center of the second half of the scattering, occurs when $qR \simeq \rho'$. From Eq. (4) and the definition of $q$ this implies that the hump center is at a scattering angle such that $\sin(\theta/2) = \sqrt{F(m)}$. For example, if $m = 1.5$, the hump center is near $\theta \simeq 34°$.

We now define the partial scattering efficiency as

$$\partial Q_{\text{sca}} = \partial C_{\text{sca}}/G, \tag{5}$$

where $G$ is the projected area of the particle onto a plane perpendicular to the incident direction. With this, one can consider the effects of absorption due to a non-zero imaginary part of the refractive index. In recent work [11] we showed that the parameter $\kappa kR$ was universal in its ability to describe when the imaginary part of the refractive index $\kappa$ has a significant effect on the scattering. When $\kappa kR \ll 1$, there is no effect; when $\kappa kR > 1$, the effect is significant. The physical basis for $\kappa kR$ is that it is the ratio of the sphere radius to the penetration skin depth of the light.

Figure 5, upper half, shows the partial scattering efficiency plotted versus $qR$ for a large, refractive particle such that $\rho' = 141$. The lower half plots the normalized differential scat-

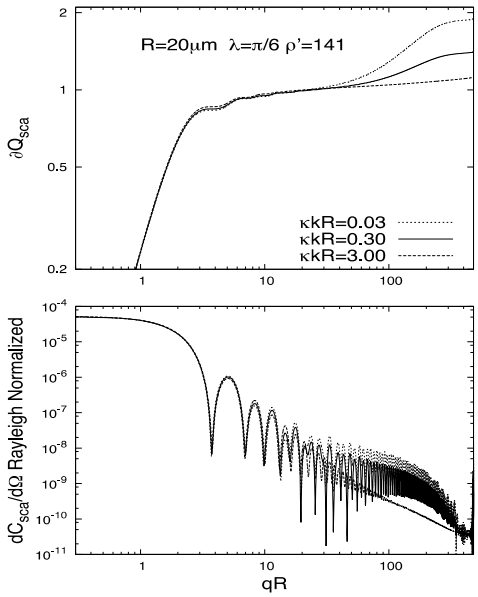


**Fig. 5.** Upper half: the partial scattering efficiency, $\partial Q_{\text{sca}}$, versus $qR$ for three spheres with $\rho' = 141$ but different values of $\kappa kR$. Lower half: Rayleigh normalized differential scattering cross section versus $qR$ ($qR$ scale matched with the upper half) for the same three spheres.

tering cross section versus the same $qR$. Three different values of the fundamental parameter $\kappa kR$ are plotted: small, crossover, and large; $\kappa kR = 0.03$, 0.3, and 3, respectively. With increasing $\kappa kR$, the lower half shows how the hump at the 2D diffraction to 3D diffraction crossover disappears. Now recall conclusion 2, above, that approximately half the scattered light comes from this region. The implication of these two statements is that with increasing $\kappa kR$, the loss of the 2D diffraction to 3D diffraction crossover will cause the total scattering to decrease by factor of 2. And indeed, the far right side of the upper half shows how the *total* scattering efficiency, which is the value of the partial scattering efficiency at the largest value of $qR$ (which corresponds to $\theta_p = 180$), evolves from a value of $\sim 2$ to a value of $\sim 1$ as $\kappa kR$ evolves from small to large.

A moment's thought sees the logical consequence to this. A large, refractive particle has an *extinction* efficiency of 2. The extinction efficiency is the sum of the scattering and absorption efficiencies. Thus when absorption is small, as indicated by $\kappa kR \ll 1$, the total scattering efficiency equals the extinction efficiency, which is 2. However, when the absorption is large, as indicated by $\kappa kR > 1$, the absorption efficiency is 1. Thus the total scattering efficiency must fall to 1 because the extinction efficiency remains equal to 2.

The results above apply to spherical particles. Here we speculate on their applicability to non-spherical particles. Non-spherical particles will have a forward scattering lobe similar to spherical particles defined within the angle $\lambda/D$ where $D$ is now a characteristic length scale of the particle. Recent results for a variety of non-spherical particles indicate that the forward scattered intensity within this angle is well described by the Rayleigh scattering divided by $\rho'^2$ [12–15]. Thus we expect that like spherical particles nearly one half of the scattered light will appear in the forward scattering lobe. This conclusion is the same as that given by Borovoi whose analysis was independent of particle shape [6]. However, dusts [9,16], perturbed spheres [13], and fractal aggregates [12] (which remain if the $\rho' < 1$ limit) do not display a hump. Thus the second half of the scattering cannot be ascribed to a hump for these shapes. On the other hand, ice crystals have a hump that disappears as $\kappa kR$ passes through unity similar to spheres [15]. Thus we can speculate that these shapes would have the other half of the light scattered within the hump.

In conclusion, the partial scattering cross section and partial scattering efficiency demonstrate that the total scattering is the sum of two roughly equal parts; approximately half comes from the forward scattering lobe, which for large refractive particle is due to 2D Fraunhofer diffraction by the sphere, and the other half from the hump at the 2D–3D Fraunhofer diffraction crossover. The first part is at angles such that $\theta \lesssim \lambda/D$, which can be quite small for large particles like those occurring in coarse mode aerosols. This is an important fact for future experiments, application of scattering for climate modeling, and construction of instruments such as nephelometers. The second part is in the hump region where $\frac{1}{2}\rho' \lesssim qR \lesssim 2\rho'$, and it disappears when the imaginary part of the refractive index is significant as indicated by $\kappa kR$.

**Funding.** National Science Foundation (NSF) (AGM 1261651); Army Research Laboratory (ARL) (W911NF-14-1-0352).

## REFERENCES

1. H. Moosmuller and W. P. Arnott, "Angular truncation errors in integrating nephelometry," Rev. Sci. Instrum. **74**, 3492–3501 (2003).
2. C. M. Sorensen, "Q-space analysis of scattering by particles: a review," J. Quant. Spectrosc. Radiat. Transfer **131**, 3–12 (2013).
3. W. R. Heinson, A. Chakrabarti, and C. M. Sorensen, "A new parameter to describe light scattering by an arbitrary sphere," Opt. Commun. **356**, 612–615 (2015).
4. W. R. Heinson, A. Chakrabarti, and C. M. Sorensen,"Crossover from spherical particle Mie scattering to circular aperture diffraction," J. Opt. Soc. Am. **31**, 2362–2364 (2014).
5. L. Brillouin, "The scattering cross section of spheres for electromagnetic waves," J. Appl. Phys. **20**, 1110–1125 (1949).
6. A. G. Borovoi, "Light scattering by large particles: physical optics and the shadow-forming field," in *Light Scattering Reviews*, A. A. Kokhanovsky, ed. (Springer-Praxis, 2013), Vol. **8**, pp. 115–138.
7. C. F. Bohren and D. R. Huffman, *Absorption and Scattering of Light by Small Particles* (Wiley, 1983).
8. M. I. Mishchenko, L. D. Travis, and A. A. Lacis, *Scattering, Absorption, and Emission of Light by Small Particles* (Cambridge University, 2002).
9. Y. Wang, A. Chakrabarti, and C. M. Sorensen, "A light-scattering study of the scattering matrix elements of Arizona Road Dust," J. Quant. Spectrosc. Radiat. Transfer **163**, 72–79 (2015).
10. Y. W. Heinson, A. Chakrabarti, and C. M. Sorensen, "A light-scattering study of Al2O3 abrasives of various grit sizes," J. Quant. Spectrosc. Radiat. Transfer **180**, 84–91 (2016).
11. G. Wang, A. Chakrabarti, and C. M. Sorensen, "Effect of the imaginary part of the refractive index on light scattering by spheres," J. Opt. Soc. Am. **32**, 1231–1235 (2015).
12. C. M. Sorensen, "Light scattering from fractal aggregates. A review," Aerosol Sci. Technol. **35**, 648–687 (2001).
13. C. M. Sorensen, E. Zubko, W. R. Heinson, and A. Chakrabarti, "Q-space analysis of scattering by small irregular particles," J. Quant. Spectrosc. Radiat. Transfer **133**, 99–105 (2014).
14. J. B. Maughan, A. Chakrabarti, and C. M. Sorensen, "Q-space analysis of light scattering by Gaussian random spheres," J. Quant. Spectrosc. Radiat. Transfer **174**, 14–21 (2016).
15. Y. W. Heinson, J. B. Maughan, J. Ding, A. Chakrabarti, P. Yang, and C. M. Sorensen, "Q-space analysis of light scattering by ice crystals," J. Quant. Spectrosc. Radiat. Transfer **185**, 86–94 (2016).
16. Y. Wang, J. Maughan, W. R. Heinson, A. Chakrabarti, and C. M. Sorensen, "Light scattering Q-space analysis of irregularly shaped particles," J. Geophys. Res. **121**, 682–691 (2016).